RSC Advances

PAPER

View Article Online
View Journal | View Issue

Cite this: *RSC Adv.*, 2023, **13**, 8923

Synthesis of temperature- and humidity-induced dual stimulation film PU-PNIPAm$_n$ and its independent film formation as a smart window application†

Jing Tian, Chengguo Jin, Xudong Wu, Cong Liao, Jiangping Xie and Yajun Luo*

Received 17th December 2022
Accepted 1st February 2023

DOI: 10.1039/d2ra08052d

rsc.li/rsc-advances

Dynamic windows, which switch between transparent and opaque states as the temperature changes, can be applied in buildings to reduce building energy consumption. Poly(*N*-isopropylacrylamide) (PNIPAm) is the most studied thermochromic hydrogel for climate-resilient smart window applications. In addition to its poor mechanical properties and low reaction rate, the PNIPAm hydrogel must be sandwiched between two pieces of glass to form an interlayer in practical applications. Here, durable PU-PNIPAm$_n$ copolymers for smart windows were synthesized by reacting the synthesized poly-NIPAm diols with isocyanate (–NCO) monomer, which greatly improved the mechanical properties of the hydrogel and it was able to form a film alone. These temperature-sensitive films can switch between transparent (>80% transmittance) and opaque (<5% transmittance) states in less than 10 minutes, with no degradation in optical contrast, switching speed, or uniformity after at least 100 switching cycles.

1 Introduction

With the growth of the population, the amount of energy used for air conditioning to provide a comfortable and livable environment has increased rapidly. Smart windows can dynamically and reversibly adjust the amount of solar radiation entering a building in response to external stimuli, providing a promising solution for improving energy efficiency.[1–6]

Current research on smart windows focuses on stimulus-responsive hydrogel materials, whose modulation process can be automatically regulated by active responses to external stimuli (*e.g.*, voltage input) or passive responses to the surrounding environment (*e.g.*, sunlight intensity, temperature, and humidity).[7–9] The simple construction of automatic passive mode responsive smart windows is usually more suitable for architectural applications than active mode, which is usually achieved using phase-separated thermochromic hydrogels with high coloring efficiency and contrast ratios.[3]

Poly(*N*-isopropylacrylamide) (PNIPAm) is a widely explored thermochromic hydrogel with a low critical solution temperature (LCST) of about 32 °C in aqueous solution, close to room temperature.[10,11] When the ambient temperature is lower than T_{LCST}, sunlight can pass through the window smoothly because of the formation of a single phase due to the hydrogen bond between the amide group and water. When the temperature rises above the T_{LCST}, the hydrogel becomes opaque due to the dominant hydrogen bonding within the polymer molecule, blocking the sunlight entering the building over the entire wavelength range.

Usually, the PNIPAm-based smart windows were established *via* sandwiching PNIPAm hydrogel thin film between two pieces of glasses to reduce water evaporation.[12,13] This makes the design and installation of smart windows more complex and invariably increases the final installation cost. This not only increases the cost of window preparation, but also places high demands on window sealing. In addition, the mechanical properties of hydrogel are poor and the size of the sandwich will shrink after a period of use, affecting the efficiency and appearance of the smart windows. These drawbacks of PNIPAm-based smart windows severely limit their commercial application.

In order to broaden the industrial application of PNIPAm-based smart windows, several important requirements need to be fulfilled:

Low cost and easy to manufacture in large areas.

Easy to transport and simple to install.

Long-term reversibility and reproducibility.

Quickly switch between transparent and opaque.

Homogeneously stable materials both above and below the T_{LCST}.

Polyurethanes (PUs) are a special class of polymeric materials that have been widely applied in biomedical, building construction, automotive, textiles and many other industries

Department of Materials and Chemical Engineering, Yibin University, Yibin 644007, PR China. E-mail: 87421239@qq.com

† Electronic supplementary information (ESI) available. See DOI: https://doi.org/10.1039/d2ra08052d

due to their superior performance in hardness, elongation, adhesives, strength, modulus, *etc.*[14–16] In order to improve the strength and modulus of PNIPAm and thus broaden its practical applications. Interestingly, the work of C. W. Park's group first demonstrated that the compressive strength of PNIPAm could be increased by more than 100% when 10% PU was added to the polymer.[17] Subsequently, scientists A. S. Mathews[18] and M. Enomoto[19] *et al.* also synthesized PNIPAm-co-PU copolymers for controlled urea release and waterproof fabrics for sportswear, respectively. However, scientists did not systematically study the mechanical and temperature–sensitive properties of these copolymers or apply them to smart windows.

In order to increase the strength and modulus of PNIPAm and thus broaden its practical application. In this paper, poly-NIPAm diols are incorporated in the first step of polyurethane synthesis to form polyurethane groups, which are produced by the reaction of alcohols (–OH) and isocyanates (–NCO). The formation of PU-PNIPAm$_n$ copolymer overcomes the defect that the hydrogel can only be encapsulated as an interlayer material to be used as a smart window, and its mechanical properties are far stronger than those of PNIPAm-based hydrogels. Furthermore, so far, this is the first study focused on the synthesis and characterization of PU-PNIPAm$_n$ copolymers for potential application as a smart window.

2 Experimental section

2.1 Materials

5-Isocyanato-1-(isocyanatomethyl)-1,3,3-trimethylcyclohexane (IPDI) and trimethylolpropane tris(2-methyl-1-aziridine) propionate (AZ) were purchased from Wanhua polyurethane Co., LTD (Yantai, China). Polyethylene glycol (PEG, $M_n = 1000$ g mol^{-1}) was supplied by Shanghai Chemical Reagent Co. Inc., China and dehydrated under reduced pressure at 100–120 °C for 3–4 h. Butane-1,4-diol (BDO) and 3-hydroxy-2-(hydroxymethyl)-2-methylpropanoic acid (DMPA) were purchased from Chengdu Kelong Co. Ltd, China and dried under vacuum at 100 °C. Acetone, butanone, oxolane (THF), [dibutyl(dodecanoyloxy)stannyl] dodecanoate (DBTDL), 2-sulfanylethanol (β-ME), diethyl ether and other common reagents were purchased from Chengdu Kelong Co. Ltd, China and were used as received. *N*-Isopropylacrylamide (NIPAm, ≥98%) and analytical grade 2-[(2-cyano-5-hydroxypentan-2-yl)diazenyl]-5-hydroxy-2-methylpentanenitrile (ACP) were purchased from Shang Hai Chemical Reagent Co. Inc., China and were used as received.

2.2 Methods

2.2.1 Synthesis of poly-NIPAm diols. Three kinds of poly-NIPAm diols (labeled PNIPAm$_n$, $n = 6$, 9, 12) were synthesized by varying the amount of β-ME. The initial reagents and ratios are shown in Table 1.

All initial reagents were dissolved in 80 g THF in a 150 mL three necked flask. And the system was purged of oxygen with nitrogen for 30 min at room temperature and heated up to 70 °C with continuous magnetic stirring for 24 h. The reaction mixture was concentrated by reduced pressure distillation at 45 °C, and then added dropwise to about 200 mL of anhydrous ethyl ether and kept in a refrigerator overnight. After filtration, the crude product was dissolved in acetone, and the filtrate was concentrated by reduced pressure distillation at 45 °C and then dried in vacuum at 60 °C for 24 h to obtained pure PNIPAm$_n$. The yield of the PNIPAm$_n$ was about 96.7%. The process was illustrated in Fig. 1a.

Table 1 Compositional ratio of monomer and initial reagents

Sample	NIPAm (g)	n (NIPAm/β-ME)	ACP wt%
PNIPAm$_{12}$	15	12/1	2
PNIPAm$_9$	15	9/1	2
PNIPAm$_6$	15	6/1	2

2.2.2 Copolymerization reaction of poly-NIPAm diol and polyurethanes (PU-PNIPAm$_n$). PU-PNIPAm$_n$ were prepared by polyaddition reaction using IPDI, PNIPAm$_n$, PEG, BDO and DMPA. The calculated PNIPAm$_n$ was dissolved in 5 g acetone, and IPDI and DBTDL (DBTDL/monomers = 0.001/1, w/w) were introduced into a 250 mL three necked flask. The reaction was stirred at 85 °C for 3 h to obtain NCO end-capped PNIPAm$_n$ intermediate. Then the dehydrated PEG and DMPA were added to the flask and kept for another 3 h. After lowering the temperature of the system to 70 °C, a stoichiometric amount of BDO was added dropwise and kept for another 3 h to obtain PU prepolymers with the hydroxyl group as the molecular terminal. The viscosity was adjusted with acetone during the reaction. A series of PU-*a*PNIPAm$_n$ modified polyurethanes were obtained by adjusting the amount of PNIPAm$_n$ added, where *a* represents the mass percentage of PNIPAm$_n$ in PU-PNIPAm$_n$. The synthetic formula is shown in Table 2 and the synthetic route is shown in Fig. 1b.

2.2.3 Preparation of the PU and PU-PNIPAm$_n$ films. The 15 wt% PU or PU-PNIPAm$_n$ solution was homogeneously mixed with 0.1940 g AZ and poured onto a horizontal PTFE mold at room temperature for 72 h, then dried at 60 °C for 24 h to obtain PU and PU-PNIPAm$_n$ cross-linked films with a thickness of about 0.5 mm.

3 Results and discussion

3.1 Structural confirmation of poly-NIPAm diol (PNIPAm$_n$)

The chemical structure was determined by ^{1}H NMR spectroscopy (400 MHz, $CDCl_3$, δ). The ^{1}H NMR spectrum shows the characteristic peaks of PNIPAm$_n$, as shown in Fig. 2 (a). As can be seen from the figure, all three PNIPAm$_n$ polymers show a proton of –NH– peak at about 7.46 ppm (a), a proton of methylene peak at about 4.01 ppm (b–d) and a proton of methyl group peak at about 1.16 ppm (e), all without the characteristic peak of protons in –C=CH_2 at about 5.6 ppm,[20] demonstrating the successful synthesis of end-hydroxy PNIPAm$_n$ by ACP and β-ME.

Fig. 2b shows the FT-IR spectrum of PNIPAm$_n$ polymers and monomer NIPAm. All three PNIPAm$_n$ samples shows N–H

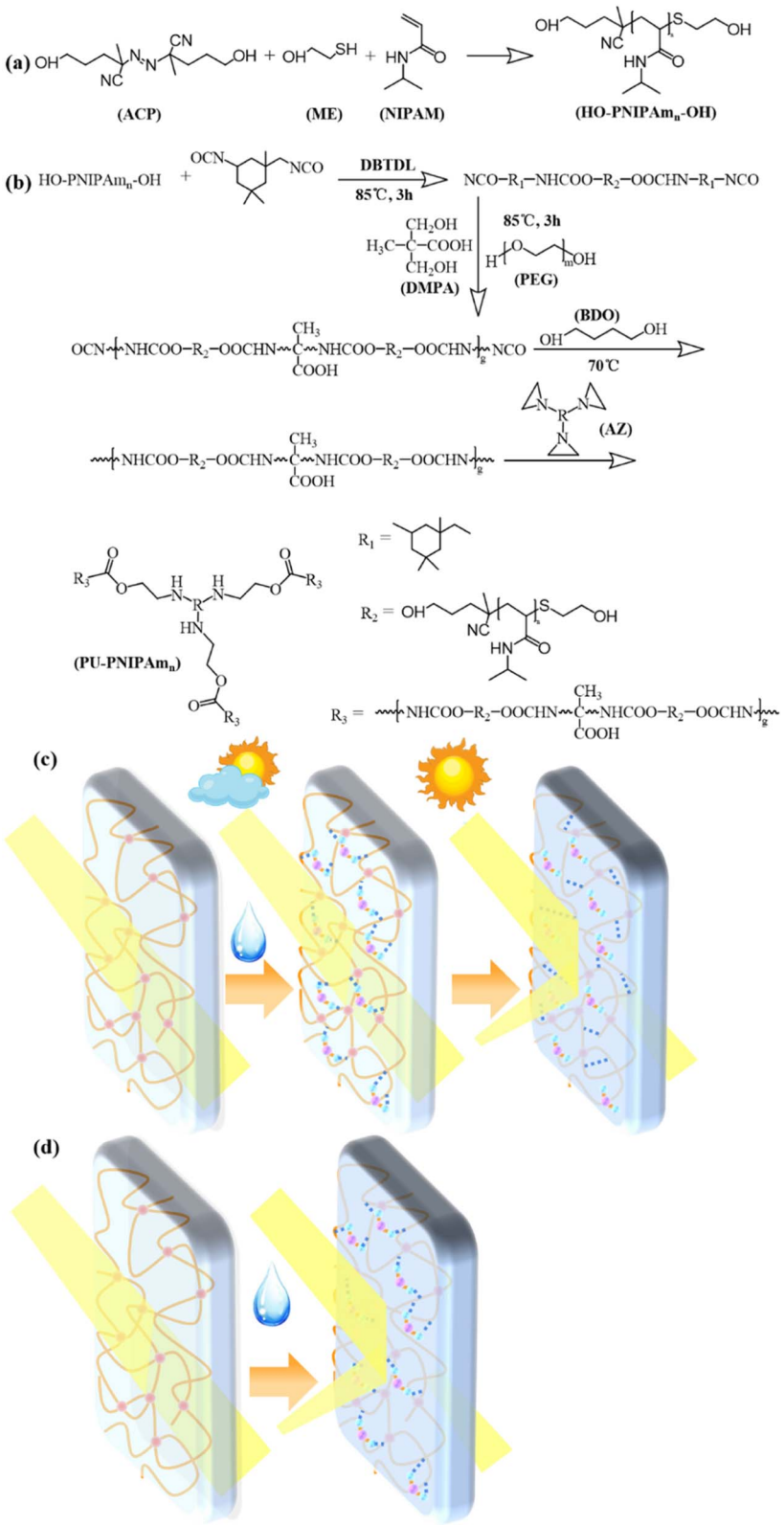

Fig. 1 Synthetic route of the PNIPAm$_n$ (a) and PU-PNIPAm$_n$ (b), (c) schematic of solar transmittance modulation of PU-0.15PNIPAm$_{12}$ and PU-0.30PNIPAm$_{12}$, (d) schematic of solar transmittance modulation of PU-0.30PNIPAm$_6$ and PU-0.30PNIPAm$_9$.

stretching vibration peaks around 3291 cm^{-1}, C=O stretching vibration peaks at 1649 cm^{-1}, and N–H bending vibration peaks at 1540 cm^{-1}. In contrast, the characteristic peaks of C=C at 1620 cm^{-1} and 987 cm^{-1} disappeared in the spectrum of PNIPAm$_n$. In addition, the peak intensity of PNIPAm$_n$ at 3438 cm^{-1} increases dramatically compared to that of NIPAm,

Table 2 Formulas of PU and PU-*a*PNIPAm$_n$

Sample	Monomer (g)						wt% (PNIPAm$_n$)
	IPDI	PEG1000	PNIPAm$_n$	DMPA	BDO	AZ	
PU	5.14	12	0	1	0.74	1.12	0
PU-0.15PNIPAm$_{12}$	5.14	9	3	1	0.74	1.12	15.00
PU-0.30PNIPAm$_{12}$	5.14	6	6	1	0.74	1.12	30.00
PU-0.45PNIPAm$_{12}$	5.14	3	9	1	0.74	1.12	45.00
PU-0.60PNIPAm$_{12}$	5.14	0	12	1	0.74	1.12	60.00
PU-0.30PNIPAm$_9$	5.14	6	6	1	0.74	1.12	30.00
PU-0.30PNIPAm$_6$	5.14	6	6	1	0.74	1.12	30.00

indicating that ME and ACP have successfully introduced hydroxyl groups into the final product. These results further demonstrated the successfully synthesis of PNIPAm$_n$.

In order to investigate the effect of PNIPAm$_n$ with different main chain lengths (different molecular weights) on the properties of PU, the molecular weights of PNIPAm$_n$ were controlled by adjusting the amount of β-ME. As the molecular weight of PNIPAm$_n$ is too large, it will increase the difficulty of copolymer synthesis; too small molecular weight not only makes the separation and purification of the product difficult, but also the addition of a large amount of β-ME makes the molecular weight distribution of PNIPAm$_n$ wider. Therefore, the average molecular weight size of PNIPAm$_n$ designed in this paper is in the range of 1000–5000. By fixing the amount of initiator ACP, the molar ratios of NIPAm to ME were designed as 12 : 1, 9 : 1 and 6 : 1, and three molecular weight sizes and distributions of PNIPAm$_n$ were produced. The molecular weight of PNIPAm$_n$ was determined by GPC, and the results are shown in Table 3. The results showed that the molecular weight of PNIPAm$_n$ decreased gradually with the increase of β-ME content, and the molecular weight distribution also became wider. This is because the higher content of β-ME, the easier it is to terminate the polymerization reaction by free radical collision, resulting in a product with a small molecular weight and a wider molecular weight distribution.[20,21]

Table 3 Molar mass and molecular distribution of PNIPAm$_n$ samples

Sample	M_n	M_w	M_w/M_n
PNIPAm$_{12}$	1776	4643	2.614
PNIPAm$_9$	1614	3854	2.388
PNIPAm$_6$	993	3157	3.180

3.2 Preparation of PU-PNIPAm$_n$ composite materials

The structure of PU-PNIPAm$_n$ films were confirmed by ^{1}H-NMR and FT-IR analysis, as shown in Fig. 3. In the ^{1}H-NMR spectrum of Fig. 3a, the attribution chemical shifts of protons in PU-PNIPAm$_n$ were labelled, preserving essentially all the peaks of PNIPAm$_n$. The peaks associated with the presence of protons in the urethane bond of PU-PNIPAm$_n$ at 7.52 ppm (a + h) and 6.99 ppm (d), demonstrating that PU-PNIPAm$_n$ was successfully synthesized by bulk polymerization of PNIPAm$_n$ and IPDI.[22]

In the FT-IR spectrum of Fig. 3b, all samples revealed strong N–H bending bond at 1533 cm^{-1}, N–H stretching bond at 3294 cm^{-1} and C=O stretching at 1710 cm^{-1} demonstrating the successful synthesis of the PU structures. In addition, the characteristic absorption peaks of isocyanate from IPDI at 2256 cm^{-1} and hydroxyl group from PEG or PNIPAm at 3440 cm^{-1} disappeared, indicating the involvement of isocyanate and hydroxyl group in the reaction. These results suggest

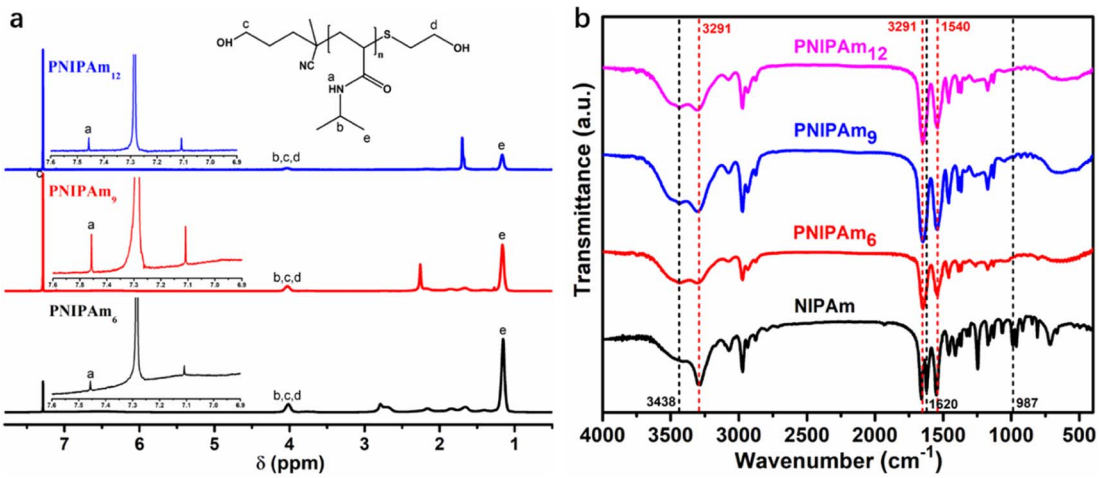

Fig. 2 (a) ^{1}H-NMR ($CDCl_3$) and (b) FT-IR spectrum of PNIPAm$_n$.

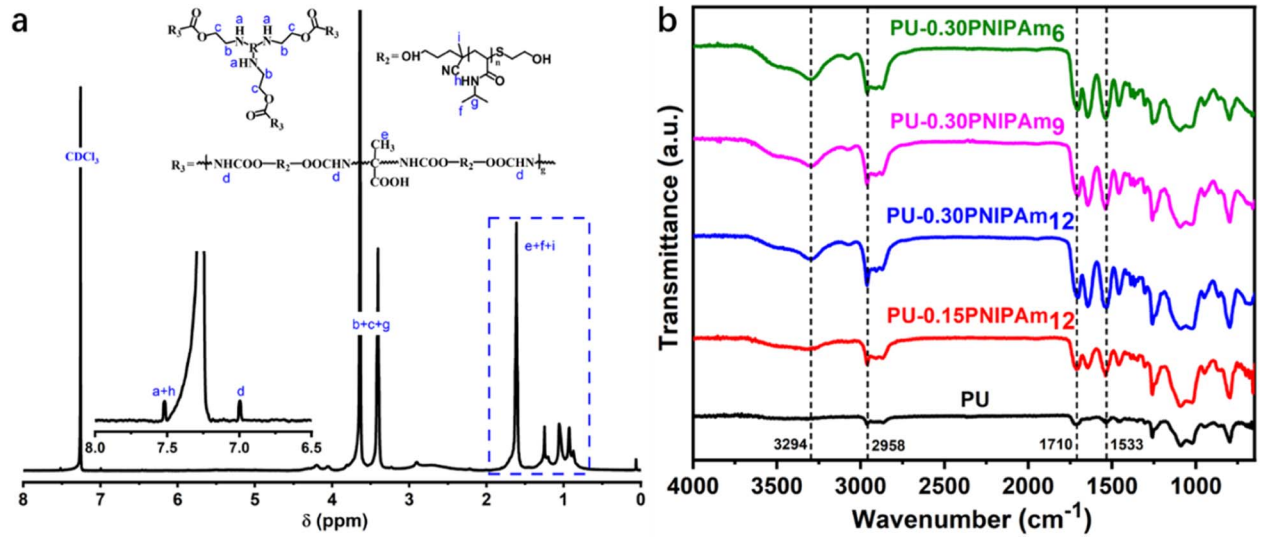

Fig. 3 (a) ^{1}H-NMR ($CDCl_3$) spectrum of PU-0.30PNIPAm$_{12}$ and (b) FT-IR spectrum of PU-PNIPAm$_n$.

that the PU-PNIPAm$_n$ copolymer was successfully prepared from PNIPAm.

PU is known to be a block copolymer consisting of alternating soft and hard segments. Under certain conditions, the hard segments in the PU chain segments will aggregate together to form crystalline micro-regions, which can be characterized by X-ray diffraction (XRD).[23,24] Fig. 4a and b presents the XRD patterns of PU and PU-PNIPAm$_n$ films. All samples showed a strong diffraction peak at around $2\theta = 19°$, caused by the crystallinity in the hard domain.[23,24] The peak intensity of these films decreased sharply with the increasing of PNIPAm$_{12}$ content and decreased slightly with the increasing of PNIPAm$_n$ molecular weight. This means that as the PNIPAm$_n$ content or molecular weight increases, lower long-range order segments are formed in the hard segment. When both PU-0.15PNIPAm$_{12}$ and PU-0.30PNIPAm$_{12}$ were swollen 100 times, their strength at $2\theta = 19°$ decreased slightly due to the stretching of the polymer chains after swelling, which reduced the long-range order of the hard segment (Fig. 4c and d).

All samples were tested by DSC after sufficient swelling in deionized (DI) water. As shown in Fig. 5a, the LCST of PNIPAm$_6$, PNIPAm$_9$ and PNIPAm$_{12}$ were 28.95 °C, 32.69 °C and 36.78 °C, respectively. The LCST of the PNIPAm$_n$ gradually increased with increasing the molecular weight, which was consistent with the results reported previously.[25,26]

As shown in Fig. 5b, the LCST of PU-0.15PNIPAm$_{12}$, PU-0.30PNIPAm$_{12}$, PU-0.30PNIPAm$_9$ and PU-0.30PNIPAm$_6$ were 70.83 °C, 62.79 °C, 57.47 °C and 54.07 °C, respectively. Compared with pure PNIPAm$_6$, the presence of many hydrophilic groups promoted the formation of hydrogen bonds, which led to a much higher LCST of the copolymers.[10] However, the LCST of PU-PNIPAm$_n$ were directly related to the molecular weight of PNIPAm$_n$, and inversely proportional to the amount of PNIPAm$_n$. Among them, the LCST of PU-0.30PNIPAm$_9$ and PU-0.30PNIPAm$_6$ with temperature sensitive effect were both lower than 60 °C, so 60 °C was chosen as the test temperature for later UV-vis-NIR test.

3.3 Thermal stabilities of PU-PNIPAm$_n$ composite materials

Thermogravimetric analysis was performed to investigate the thermal stability of PU-PNIPAm$_n$ films. The TGA and DTG curves of PU and PU-PNIPAm$_n$ are presented in Fig. 6 and the details were summarized in Table 4. All samples presented two stages of decomposition in the region of 160–469 °C, a very slight decomposition due to the thermal degradation of urethane bonds in hard segments, while the other major degradation assigned to the degradation of PEG and PNIPAm$_n$ chains scission of soft segments.

The TGA curves shows that the temperature of 5% weight loss ($T_{-5\ wt\%}$) of all samples decreases gradually with increasing PNIPAm$_n$ content (Fig. 6a) or molecular weight (Fig. 6c), indicating that the thermal stability of PU-PNIPAm$_n$ decreases with increasing PNIPAm$_n$ content or molecular weight. This result is consistent with the results of XRD in the previous Fig. 4.

As can be seen from the DTG curves, the main thermal decomposition temperature T_{max2} of all samples increases progressively with increasing PNIPAm$_n$ content (Fig. 6b) and molecular weight (Fig. 6d). This decomposition stage is mainly attributed to the thermal degradation of the soft segments, as expected.

The decomposition temperature (T_{max1}) increased sharply with increasing PNIPAm$_{12}$ content, but decreased slightly with increasing PNIPAm$_n$ molecular weight. This may be due to the fact that when the content of PNIPAm$_{12}$ increases, hydrogen bonds tend to form between the molecular chains, thus increasing the decomposition temperature of the hard segment.[18,27] When the same amount of PNIPAm$_n$ is added, the decomposition temperature of the hard segment decreases as the molecular weight increases, due to the formation of lower long-range order segments in the hard segments.[20,27]

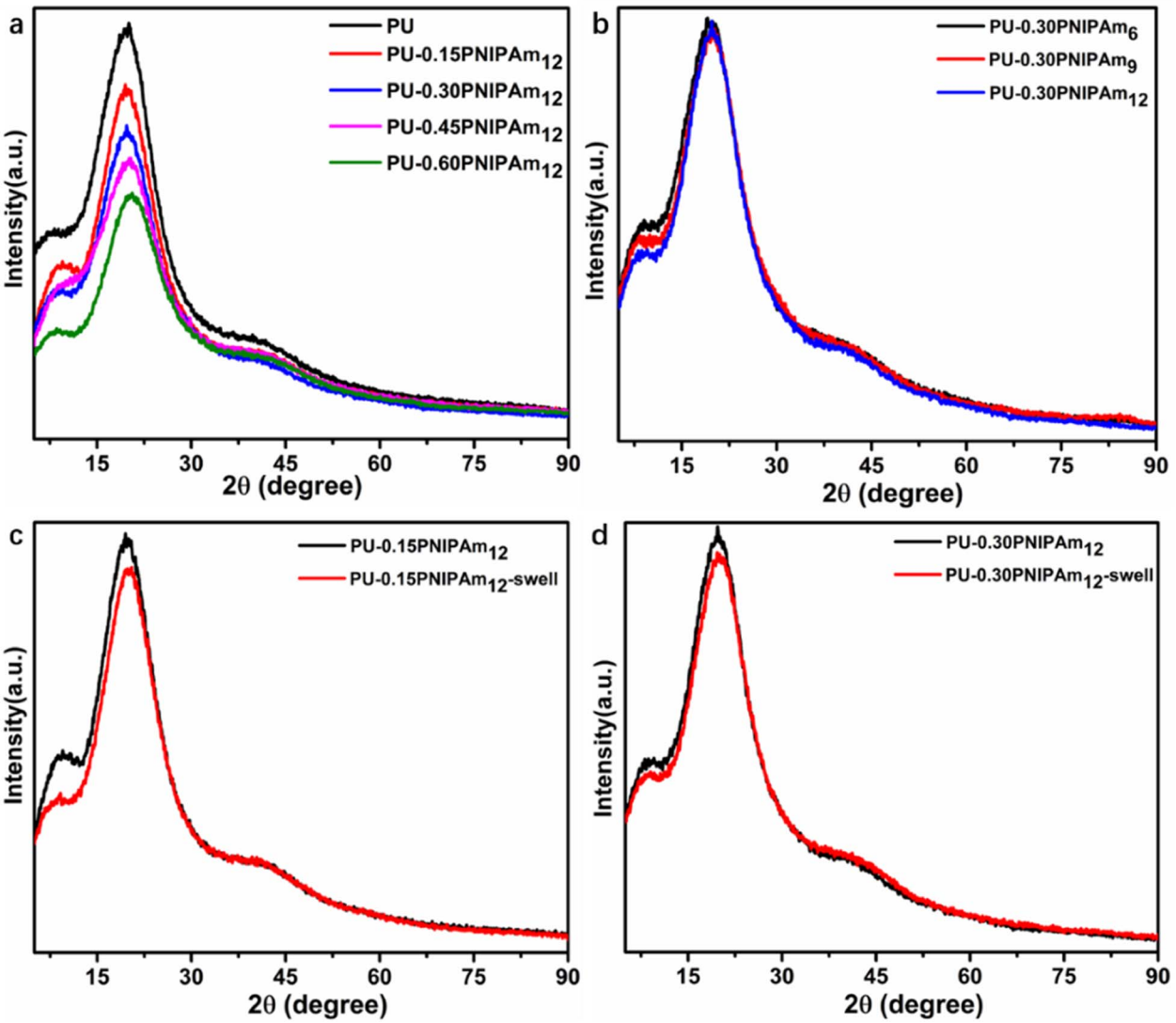

Fig. 4 XRD patterns of the PU and PU-PNIPAm$_n$ films. (a) PU-*a*PNIPAm$_{12}$, (b) PU-0.30PNIPAm$_n$, (c) PU-0.15PNIPAm$_{12}$ before and after swelling, (d) PU-0.30PNIPAm$_{12}$ before and after swelling.

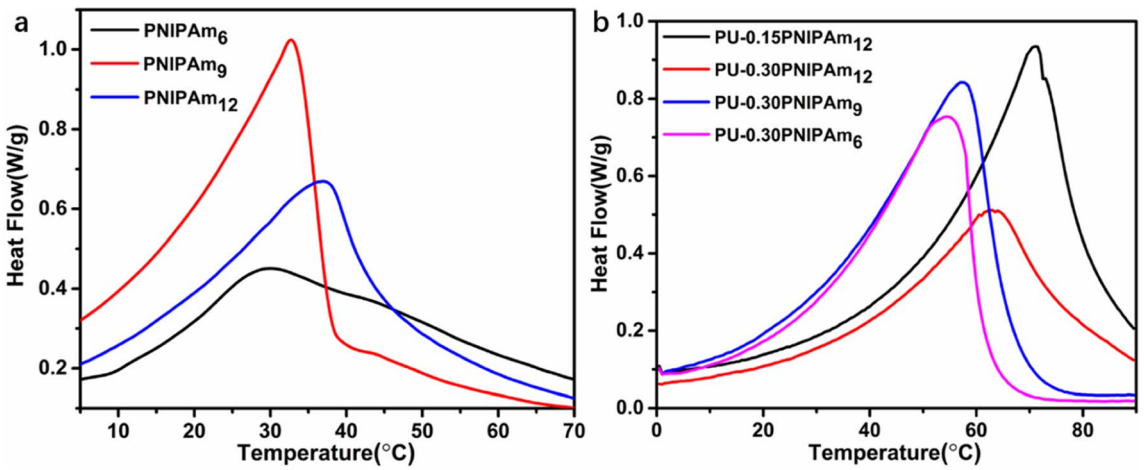

Fig. 5 DSC of all samples. (a) PNIPAm$_n$, (b) PU-*a*PNIPAm$_n$.

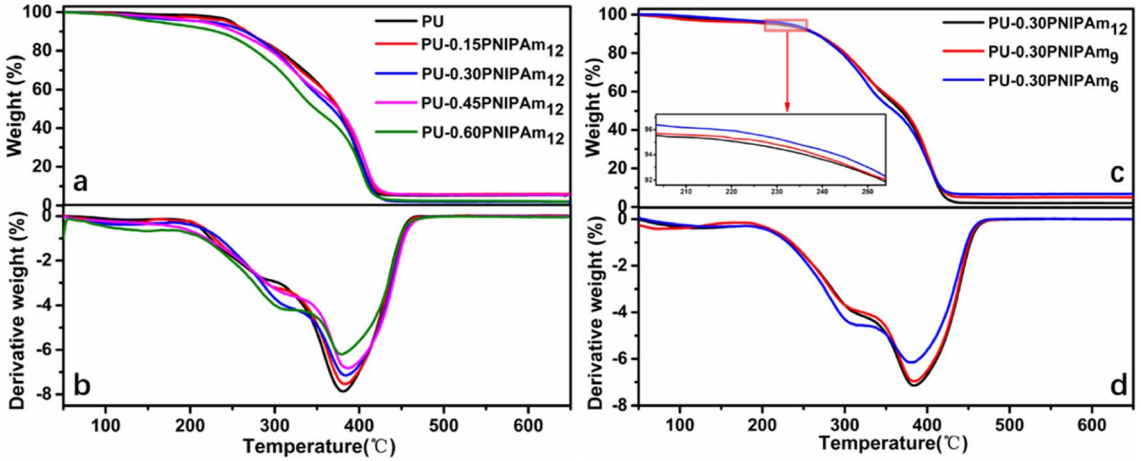

Fig. 6 The thermal stabilities of the PU and PU films: (a and c) TGA and (b and d) DTG curves.

Table 4 Thermal stabilities of the PU and PU-PNIPAm$_n$ films

Sample	$T_{-5\ wt\%}$ (°C)	T_{max1} (°C)	T_{max2} (°C)	Residual mass (%)
PU	249.20	290.77	381.33	5.25
PU-0.15PNIPAm$_{12}$	243.91	301.03	383.65	5.81
PU-0.30PNIPAm$_{12}$	221.97	307.31	384.04	2.02
PU-0.45PNIPAm$_{12}$	214.56	309.64	386.79	5.60
PU-0.60PNIPAm$_{12}$	161.63	311.96	378.18	2.39
PU-0.30PNIPAm$_9$	227.59	308.14	383.62	4.97
PU-0.30PNIPAm$_6$	233.74	311.29	380.37	6.68

These results indicated that the thermal stability of PU-PNIPAm$_n$ films is worse than that of PU due to the wide molecular weight distribution of PNIPAm$_n$ resulting in the low regularity of PU. However, the minimum initial decomposition temperature of all films is 161 °C, which is sufficient for practical application of the smart window.

3.4 Mechanical properties and microstructure analysis

In general, the tensile strength of the polymer matrix plays a key role in the mechanical properties of PU-PNIPAm$_n$ films. Fig. 7a shows the typical stress–strain curves of PU-PNIPAm$_n$ films with different content of PNIPAm$_n$. As well as tensile strength, elongation at break, Young's modulus and toughness values are summarized in Table 5. Comparatively with the pure PU, the ultimate tensile strengths (stress at break), the elongations and the toughness were increased dramatically by increasing the content of PNIPAm$_{12}$. For example, compared with pure PU, the tensile strength, elongation at break and toughness of PU-0.30PNIPAm$_{12}$ increased by 346.8%, 416.9% and 1047.1%, respectively.

These results are attributed to two effects. On the one hand, the molecular weight of PNIPAm$_n$ is much larger than 1000, which increases the flexibility of the soft segment, and the higher the molecular weight, the greater the flexibility.[28] On the other hand, the increase in PNIPAm$_n$ content leads to an increase in intermolecular hydrogen bonding, allowing the

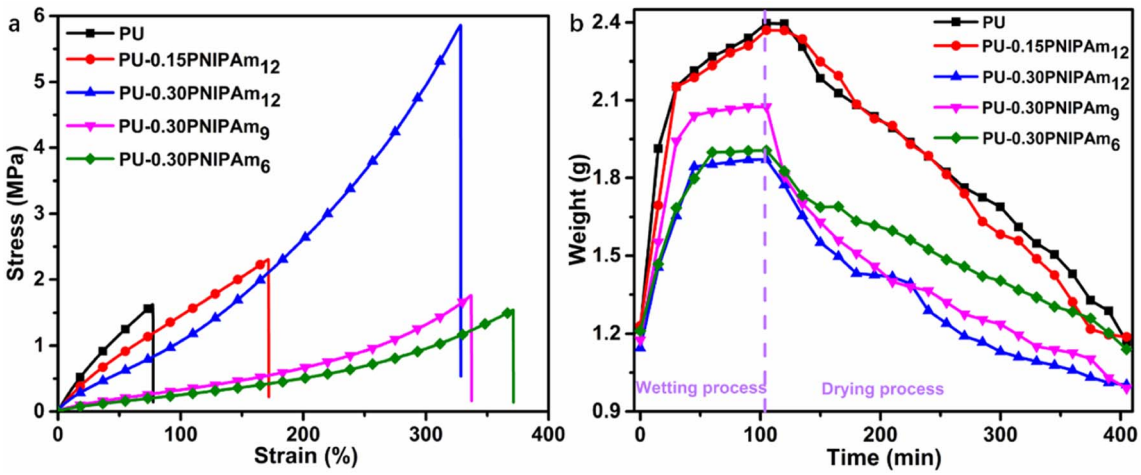

Fig. 7 (a) The tensile stress–strain curves and (b) weight changes of PU-PNIPAm$_n$ films.

Table 5 Mechanical properties of PU-PNIPAm$_n$ films

Sample	Stress (MPa)	Strain (%)	Modulus (MPa)	Toughness (MJ m^{-3})
PU	1.56 ± 0.12	79.86 ± 6.49	3.29 ± 0.17	0.70 ± 0.10
PU-0.15PNIPAm$_{12}$	2.29 ± 0.02	159.36 ± 12.5	2.39 ± 0.16	2.00 ± 0.16
PU-0.30PNIPAm$_{12}$	5.41 ± 0.40	332.94 ± 6.10	2.18 ± 0.37	7.33 ± 0.18
PU-0.30PNIPAm$_9$	1.70 ± 0.31	344.69 ± 7.5	1.13 ± 0.22	2.22 ± 0.11
PU-0.30PNIPAm$_6$	1.50 ± 0.04	369.86 ± 1.33	0.97 ± 0.06	2.01 ± 0.09

material to improve the tensile fracture strength and flexibility of the film through an energy dissipation mechanism under the action of external forces.[20,29]

It can also be seen from Fig. 7a that the tensile strength of PU-0.30PNIPAm$_n$ decreases with the decrease of PNIPAm$_n$ backbone length, which is due to the decrease of interaction between hard segments, resulting in the microphase separation and the decrease of crystallinity of hard segments. While the elongations and the toughness were increased with decreasing PNIPAm$_n$ backbone length due to the increase of hydrogen bond carbonyl content in hard segments.

Since thermochromic PU-PNIPAm$_n$ films need to absorb a certain amount of water in order to function. Therefore, a 4 × 4 cm PU-PNIPAm$_n$ membrane was immersed in deionized water to study the time required to reach swelling equilibrium, and the results are shown in Fig. 7b. As can be seen from the figure, all samples reached swelling equilibrium in nearly 105 min. The shortest time to reach swelling equilibrium is PU-0.30PNIPAm$_{12}$, which was about 45 min. After the samples reached the swelling equilibrium, they were removed from water and placed in air, and the weight changes of all the films are shown in Fig. 7b. It takes about 300 min for the PU films to dry out after the swelling equilibrium, regardless of the weather factor. Therefore, this temperature-sensitive PU film can be applied to smart windows.

3.5 Transmittance modulation by PU-PNIPAm$_n$ devices

To investigate the effect of different molecular weights and dosages of PNIPAm$_n$ in films on the solar light regulation ability, the UV-vis-NIR transmittance spectra (200–2500 nm) of all samples are shown in Fig. 8a. As shown in Fig. 8, there are two more transmittance valleys after swelling than before, at approximately 1430 nm and 1930 nm, indicating typical O–H stretching and a combination of O–H stretching and H–O–H bending of water.[30] PU, PU-0.30PNIPAm$_6$ and PU-0.30PNIPAm$_9$ have higher optical transmission in the swollen state than in the dry state, which is due to a slight increase in volume of the material after swelling in water and increase in intermolecular pores, thus increasing the optical transmittance.

As shown in Fig. 8a, PU-0.15PNIPAm$_{12}$ and PU-0.30PNIPAm$_{12}$ are sensitive to humidity and can change from colored opaque state to transparent state by adsorption/desorption of water. Both films exhibit a high transmittance transparent state in the dry state, while the transmittance decreases sharply in the swollen state. As shown in Table 6, before and after swelling, ΔT_{lum}, ΔT_{IR} and ΔT_{Sol} were 17.24%, 26.86%, and 22.93% for PU-0.15PNIPAm$_{12}$ and 34.10%, 42.63%, and 38.96% for PU-0.30PNIPAm$_{12}$, respectively. Both types of films are hydrochromic because the film absorbs water, which causes the polymer chains to stretch, causing the polymer chains to lose directionality and thus form a more disordered network, increasing the random scattering of sunlight by the polymer chains and leading to a decrease in light transmission.[31] In summary, PU-0.15PNIPAm$_{12}$ and PU-0.30PNIPAm$_{12}$ can use humidity to control solar regulation, and the regulation capacity increases with increasing amounts of PNIPAm$_{12}$. This is because when more PNIPAm$_{12}$ is introduced into PU, some molecular chains tend to aggregate and form small balls after swelling over, generating strong Michell scattering and thus reducing the light transmittance.[31,32] In addition, the color change process depends on the adsorption/desorption of water, and the coloring process

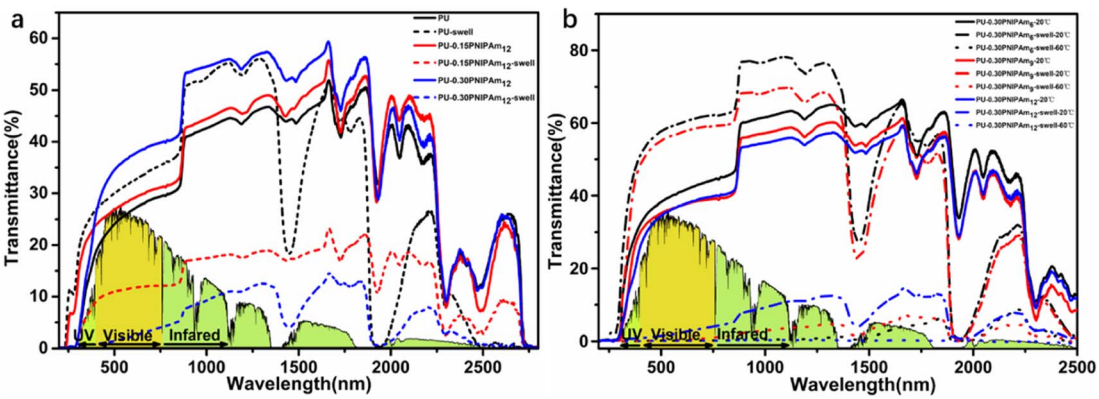

Fig. 8 (a) UV-vis-NIR transmittance spectra of PU and PU-PNIPAm$_{12}$ films at 20 °C before and after swelling; (b) UV-vis-NIR transmittance spectra of PU-0.30PNIPAm$_n$ films at 20 °C and 60 °C before and after swelling.

Table 6 Comparison of optical properties of different PU-PNIPAm$_n$ films[a,b]

Film	PU	PU-0.30PNIPAm$_6$	PU-0.30PNIPAm$_9$	PU-0.30PNIPAm$_{12}$	PU-0.15PNIPAm$_{12}$
Thickness (mm)	0.46	0.44	0.44	0.42	0.40
$T_{lum(20\ °C)}$	26.30	40.73	36.83	36.60	28.70
$T_{lum(20°C),\ swell}$	32.25	59.53	56.78	2.50	11.46
$T_{lum(60\ °C),\ swell}$	—	0.19	0.50	0.14	—
$\Delta T_{lum(1)}$	−5.95	−18.80	−19.95	34.10	17.24
$\Delta T_{lum(2)}$	—	59.34	56.28	2.36	—
$T_{IR(20\ °C)}$	41.58	58.53	53.59	51.82	43.87
$T_{IR(20°C),\ swell}$	46.70	67.34	60.63	9.19	17.01
$T_{IR(60\ °C),\ swell}$	—	1.13	3.40	0.27	—
$\Delta T_{IR(1)}$	−5.12	−8.81	−7.04	42.63	26.86
$\Delta T_{IR(2)}$	—	66.21	57.23	8.92	—
$T_{Sol(20\ °C)}$	35.24	51.14	46.61	45.42	37.63
$T_{Sol\ (20\ °C),\ swell}$	40.75	63.98	58.84	6.46	14.70
$T_{Sol\ (60\ °C),\ swell}$	—	0.74	2.22	0.22	—
$\Delta T_{Sol\ (1)}$	−5.51	−12.84	−12.23	38.96	22.93
$\Delta T_{Sol\ (2)}$	—	63.24	56.62	6.24	—

[a] $\Delta T_{lum/IR/sol\ (1)} = T_{lum/IR/sol,\ 20\ °C} - T_{lum/IR/sol,\ 20\ °C,\ swell}$. [b] $\Delta T_{lum/IR/sol\ (2)} = T_{lum/IR/sol,\ 20\ °C,\ swell} - T_{lum/IR/sol,\ 60\ °C,\ swell}$.

requires only the adsorption of water, while the bleaching process requires only the desorption of water under ambient conditions.

PU-0.30PNIPAm$_6$ and PU-0.30PNIPAm$_9$ films could not respond to humidity, but to temperature. The T_{lum} of PU-0.30PNIPAm$_6$ and PU-0.30PNIPAm$_9$ in the swollen state was relatively high at 20 °C, which are 59.53% and 56.78%, respectively. Both samples in the swollen state exhibit good thermal reactivity, which can be changed from transparent to opaque by heating, thus blocking most of the incoming light, including infrared. As shown in Fig. 8b, when the temperature rises from 20 to 60 °C, the ΔT_{lum}, ΔT_{IR} and ΔT_{Sol} were 59.34%, 66.21%, and 63.24% for PU-0.30PNIPAm$_6$ and 56.28%, 57.23%, and 56.62% for PU-0.30PNIPAm$_9$, respectively. In addition, the ΔT_{Sol} could be further improved by 6.24% when the swollen PU-0.30PNIPAm$_{12}$ was heated to 60 °C. In conclusion, PU-0.30PNIPAm$_6$ and PU-0.30PNIPAm$_9$ can use temperature to control solar regulation, and the regulation ability increases with the increase of PNIPAm$_n$ molecules. Fig. 9 shows the macroscopic photos of all the films in different states and temperatures, from which the actual situation of the films as smart windows applications can be clearly observed.

Fig. 10 shows the change in optical transparency of the PU-PNIPAm$_n$ smart window at 550 nm after 50 cycles of stimulation. After 50 cycles, the composite smart window exhibited good stability with good reversibility and repeatability of the transparent–opaque transition.

Fig. 9 The digital photographs of all samples at 20 °C (dry state, top), 20 °C (wet state, middle) and 60 °C (wet state, bottom).

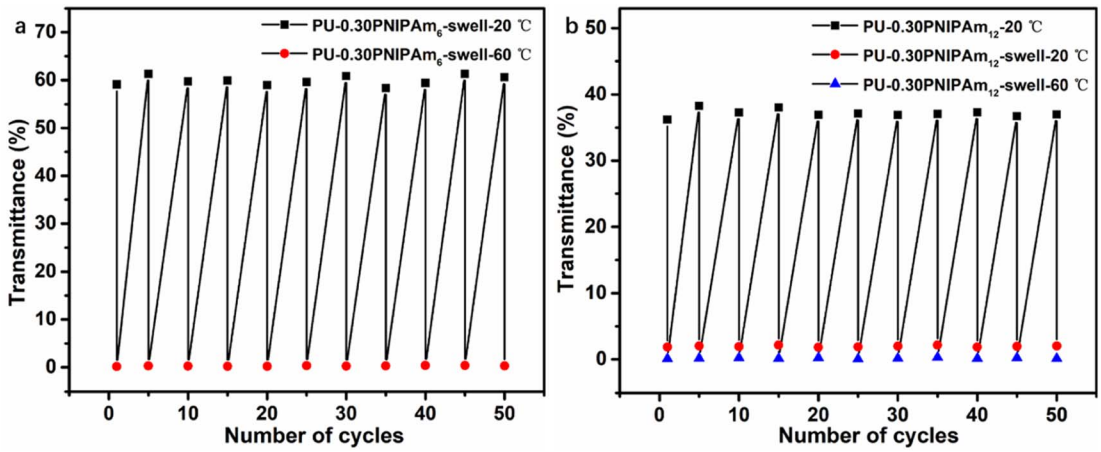

Fig. 10 Reproducibility of transmittance at 550 nm for (a) PU-0.30PNIPAm$_6$ and (b) PU-0.30PNIPAm$_{12}$ smart window.

4 Conclusion

In this paper, poly-NIPAm diols are incorporated in the first step of polyurethane synthesis to form PU-PNIPAm$_n$ copolymers. The PU-PNIPAm$_n$ copolymer greatly improves the mechanical properties of hydrogel and overcomes the defect that hydrogel can only be applied to smart windows as a sandwich material. Synthesized PU-0.15PNIPAm$_{12}$ and PU-0.30PNIPAm$_{12}$ films have hydro-chromic properties that allow solar modulation using humidity control, and the modulation ability increases with the amount of PNIPAm$_{12}$. Synthesized PU-0.30PNIPAm$_6$ and PU-0.30PNIPAm$_9$ films have thermo-chromic properties that allow solar modulation using temperature control, and the modulation ability increases with the increase of PNIPAm$_n$ molecules. Besides these PU-PNIPAm$_n$ films can switch between transparent (about 50% transmittance) and opaque (<5% transmittance) states in less than 10 minutes.

Conflicts of interest

There are no conflicts to declare.

Acknowledgements

We acknowledge the funding support from the Yibin City Science and Technology Program (2021JC004), Pre-Research Program of Yibin University (2020YY03), Sichuan Student Innovation Project (S202210641068, S202210641116).

Notes and references

1 Y. Zhou, Y. Cai, X. Hu and Y. Long, *J. Mater. Chem. A*, 2014, **2**, 13550–13555.
2 J. Tian, H. Peng, X. Du, H. Wang, X. Cheng and Z. Du, *Prog. Org. Coat.*, 2021, **157**, 106287.
3 J. Tian, J. Xu, H. Peng, X. Du, H. Wang, Z. Du and X. Cheng, *Prog. Org. Coat.*, 2021, **160**, 106531.
4 Y. Zhou, M. Layani, S. Wang, P. Hu, Y. Ke, S. Magdassi and Y. Long, *Adv. Funct. Mater.*, 2018, **28**, 1705365.
5 L. Tang, L. Wang, X. Yang, Y. Feng, Y. Li and W. Feng, *Prog. Mater. Sci.*, 2021, **115**, 100702.
6 Y. Niu, Y. Zhou, D. Du, X. Ouyang, Z. Yang, W. Lan, F. Fan, S. Zhao, Y. Liu, S. Chen, J. Li and Q. Xu, *Adv. Sci.*, 2022, **9**, e2105184.
7 M. Wu, Y. Shi, R. Li and P. Wang, *ACS Appl. Mater. Interfaces*, 2018, **10**, 39819–39827.
8 Z. Xu, S. Wang, X.-Y. Hu, J. Jiang, X. Sun and L. Wang, *Sol. RRL*, 2018, **2**, 1800204.
9 Y. Zhou, F. Fan, Y. Liu, S. Zhao, Q. Xu, S. Wang, D. Luo and Y. Long, *Nano Energy*, 2021, **90**, 106613.
10 K. Jain, R. Vedarajan, M. Watanabe, M. Ishikiriyama and N. Matsumi, *Polym. Chem.*, 2015, **6**, 6819–6825.
11 X. H. Li, C. Liu, S. P. Feng and N. X. Fang, *Joule*, 2019, **3**, 290–302.
12 Y. Zhou, S. Wang, J. Peng, Y. Tan, C. Li, F. Y. C. Boey and Y. Long, *Joule*, 2020, **4**, 1–17.
13 J. Tian, J. Gu, H. Peng, H. Wang, Z. Du, X. Cheng and X. Du, *Composites, Part A*, 2021, **149**, 106538.
14 J. O. Akindoyo, M. D. H. Beg, S. Ghazali, M. R. Islam, N. Jeyaratnam and A. R. Yuvaraj, *RSC Adv.*, 2016, **6**, 114453–114482.
15 J. G. Lundin, G. C. Daniels, C. L. McGann, J. Stanbro, C. Watters, M. Stockelman and J. H. Wynne, *Macromol. Mater. Eng.*, 2017, **302**, 1600375.
16 Y. Fang, X. Du, Z. Du, H. Wang and X. Cheng, *J. Mater. Chem. A*, 2017, **5**, 8010–8017.
17 C. W. Park, S. M. Cho and B. K. Kim, *React. Funct. Polym.*, 2006, **66**, 585–591.
18 A. S. Mathews and S. Narine, *J. Polym. Sci., Part A: Polym. Chem.*, 2010, **48**, 3236–3243.
19 M. Enomoto, Y. Omote, M. Miyajima and C. K. Yun, *Adv. Polym. Technol.*, 2018, 3737–3746, DOI: 10.1002/adv.22157.
20 W. Yang, X. Cheng, H. Wang, Y. Liu and Z. Du, *Polymer*, 2017, **133**, 68–77.
21 M. E. O'Reilly, S. Dutta and A. S. Veige, *Chem. Rev.*, 2016, **116**, 8105–8145.
22 X. Du, H. Wang, Z. Du and X. Cheng, *Thermochim. Acta*, 2017, **651**, 58–64.

23 L. Li, X. Wang, Z. Li, W. Bi, Y. Li, Y. Qi and Q. Dong, *New J. Chem.*, 2016, **40**, 596–605.
24 L. F. Wang and Y. H. Wei, *Colloids Surf., B*, 2005, **41**, 249–255.
25 Q. Duan, Y. Miura, A. Narumi, X. Shen, S.-I. Sato, T. Satoh and T. Kakuchi, *J. Polym. Sci., Part A: Polym. Chem.*, 2006, **44**, 1117–1124.
26 Z. Tong, F. Zeng and X. Zheng, *Macromolecules*, 1999, **32**, 4488–4490.
27 C. C. Lai and C. K. Chung, *Surf. Coat. Technol.*, 2020, **389**, 125606.
28 D. L. Merlin and B. Sivasankar, *Eur. Polym. J.*, 2009, **45**, 165–170.
29 S. Yang, X. Du, Z. Du, M. Zhou, X. Cheng, H. Wang and B. Yan, *Polymer*, 2020, **190**, 122219.
30 Y. Zhou, Y. Cai, X. Hu and Y. Long, *J. Mater. Chem. A*, 2015, **3**, 1121–1126.
31 M. V. Rybin, A. B. Khanikaev, M. Inoue, K. B. Samusev, M. J. Steel, G. Yushin and M. F. Limonov, *Phys. Rev. Lett.*, 2009, **103**, 023901.
32 G. Cai, J. Wang, A. L. Eh, J. Chen, K. Qian, J. Xiong, G. Thangavel and P. S. Lee, *ACS Appl. Mater. Interfaces*, 2018, **10**, 37685–37693.